RSC Advances

PAPER

View Article Online
View Journal | View Issue

Cite this: *RSC Adv.*, 2023, **13**, 22158

A novel, efficient and magnetically recyclable Cu–Ni bimetallic alloy nanoparticle as a highly active bifunctional catalyst for Pd-free Sonogashira and C–N cross-coupling reactions: a combined theoretical and experimental study†

Mohammad Ali Nasseri, * Mansoore Shahabi, Seyyedeh Ameneh Alavi G. and Ali Allahresani

Received 25th March 2023
Accepted 5th July 2023

DOI: 10.1039/d3ra01965a

rsc.li/rsc-advances

In this study, a Fe_3O_4@SiO_2@Cyt-Ni/Cu nanocomposite as a novel heterogeneous bimetallic catalyst was synthesized which exhibits efficient performance for the Sonogashira and C–N cross-coupling reactions. The characterization of the catalyst was studied by FT-IR, PXRD, VSM, EDX, TEM, FE-SEM and TGA analyses. The geometry optimization and relative energies of the designed bimetallic complexes were theoretically determined using density functional theory (DFT) calculation at the B3LYP/6-31G**/LANL2DZ level. The catalyst showed good activity in the coupling of various aryl halides with alkynes (Sonogashira reaction) as well as aryl halide with *N*-heterocycles and achieved coupling products with good to high yields for all of them in a short time. The high catalytic performance could be due to the synergistic effect between Ni and Cu, which causes the reaction to proceed more efficiently. This heterogeneous nanocatalyst could be easily recovered from the reaction mixture with an external magnet and reused for 7 consecutive runs with minimal loss of catalytic activity.

1. Introduction

The carbon–carbon and carbon–heteroatom cross-coupling reactions are important types of bond-forming reactions in organic synthesis as they lead to the formation of pharmaceutical and agrochemical products.[1–3]

Among various couplings, the Ullmann reaction for C–N synthesis is known as one of the most reliable, controllable, and widespread coupling reactions.[4,5] After the Ullmann reaction, the most robust and effective method for the formation of C(sp)–C(sp^2) bonds between aryl halides and phenylacetylene in the synthesis of phenylethynyl derivatives is the Sonogashira cross-coupling reaction, which produces valuable intermediates in the preparation of biologically active molecules, agrochemicals, pharmaceuticals, polymers and engineered materials.[6–9] These compounds are employed in molecular electronics, sensing, and optical materials.[10–13]

Traditional methods for the Sonogashira coupling reaction have been applied by homogeneous Pd catalysts.[14] In spite of the high performance and stereoselectivity of palladium catalysts, some limitations including using toxic ligands and high cost of palladium as well as difficulties in separation Pd residue from products have become crucial challenges. Therefore, researchers prefer Pd-free system due to reduction of Pd pollution, minimizing its negative environmental and economic impact effects. Thus, heterogeneous approach is a promising route to solve these problems. The heterogeneous systems have been subject of many researches due to easier handing, simple workup and reusability.[15–19]

In this context, the heterogeneous catalysts in the form of magnetic nanoparticles (MNPs) have attracted considerable attentions due to their unique properties such as ease of availability, high accessible surface area and excellent thermal stability.[20,21] In addition, these magnetic nanoparticles strongly response to magnetic field and efficiently recover from the reaction mixture by an external magnet.

Recently, low cost and easy availability metal nanoparticles such as nickel and copper have been developed as efficient catalysts for the Sonogashira cross-coupling reaction.[22–25] Thathagar *et al.* reported the Sonogashira coupling reaction of alkynes and aryl halides using copper nanoclusters catalyse in 110 °C and products isolated in good yields (80–85%) and high selectivity.[26] In addition, the excellent catalytic activity of Cu/Cu_2O nanoparticles in the Sonogashira coupling reaction of alkynes with acyl chlorides was reported.[27] Santandrea *et al.* developed a macrocyclic Cu-catalyzed Sonogashira-type cross coupling reaction which employs an operationally simple CuCl/

Department of Chemistry, Faculty of Sciences, University of Birjand, P. O. Box 97175-615, Birjand, Iran. E-mail: manaseri@birjand.ac.ir

† Electronic supplementary information (ESI) available: ^{1}H-NMR and ^{13}C-NMR spectra of coupling products. See DOI: https://doi.org/10.1039/d3ra01965a

phen/Cs_2CO_3 catalyst system.[28] The catalytic performance of NHC [CNN] pincer nickel(II) complexes with moderate to excellent yields of the Sonogashira cross-coupling products was also explored by Wang *et al.*[29] The using of Ni-PPh_2-PMOs(Ph) catalyst exhibited the highest activity and selectivity in the water-medium Sonogashira reaction.[30] The Sonogashira cross-coupling reaction has been also studied using nickel ferrite nanoparticles (NPs),[31] reduced graphene oxide supported Cu_2O nanoparticles,[32] MCM-41-immobilized Schiff base-pyridine bidentate copper(I) complex.[33]

In recent decades, bimetallic catalysts have been attracted considerable attentions in academic and industrial applications due to significant higher catalytic performance compared to their monometallic counterparts which is contributed to the electronic communication between two distinct metals.[34–38] The strong interfacial interaction between two metals provides fast electron transfer and high reaction activity. Therefore, this perspective highlights an alternative pattern for the use of bimetallic catalysts in coupling reactions.[39–42]

Cu-based catalysts have become a tremendous interest, because of their abundant reserves, low costs and considerably high catalytic activity for carbon–carbon bond formation.[43] Anyway, the presence of a second metal such as nickel due to the synergistic effect between two metals can effectively enhance performance of the catalyst. There have been numerous reports about bimetallic systems based on Ni–Cu nanoparticles for a variety of organic reactions.[44–51] Lipshutz *et al.* synthesized a heterogeneous bimetallic catalyst composed of copper and nickel oxide particles supported within charcoal (Ni/Cu@C).[51] It was the first example of a mixed-metal catalyst composed of Cu and Ni that can mediate both groups 10 and group 11 cross-couplings. *N*-Alkylation of amines with alcohols was reported with the use of Ni–Cu bimetallic nanoparticles catalyst supported on γ-Al_2O_3.[52] It was found that the Cu/Ni catalyst led to the best results in terms of both conversion and selectivity compared with monometallic NPs. Varadwaj and co-workers reported the enhancement of C–S coupling by an amine-functionalized montmorillonite-supported Cu, Ni bimetallic catalyst.[53] Krishna and co-workers synthesized Cu@Ni/rGO nanocomposite as a catalyst for reduction of 4-nitrophenol (4-NP) to 4-aminophenol (4-AP).[54] Furthermore, Cu–Ni bimetallic nanoparticles grafted on amine functionalized graphene oxide were examined towards selectivity reduction of nitro compounds as well as hydrogenation of cinnamaldehyde.[49] Nasresfahani *et al.* reported a bimetallic mesoporous system, *i.e.*, Ni/Cu-MCM-41 as a reusable and efficient bimetallic catalyst for the Sonogashira coupling of different aryl halides with phenylacetylene under palladium-free conditions.[44] They found that the bimetallic system could be successfully recovered from the reaction mixture and reused for five consecutive catalytic cycles without significant loss of its activity.

Bimetallic catalysts can perform multi-step reactions in one-pot to obtain the target product with high efficiency, high selectivity, low reaction time and elimination of intermediate purification/separation step. Therefore, energy savings and reduction of final product cost are the advantages of these

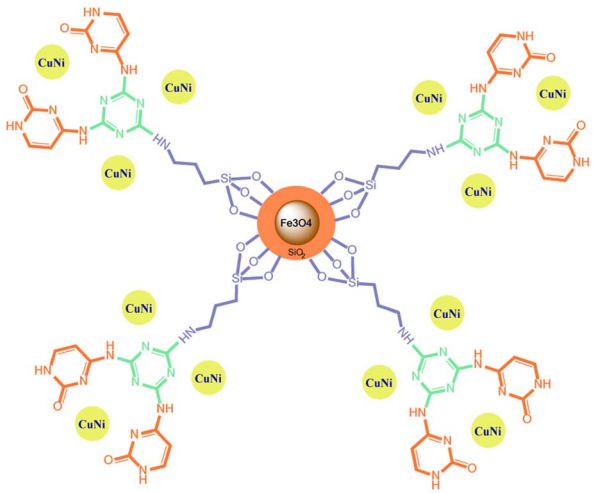

Scheme 1 Fe_3O_4@SiO_2@Cyt-Ni/Cu nanocomposite structure.

catalysts in cascading reactions. Regarding to the advantages of bimetallic magnetic nanocomposite and their high efficiency in the synthesis of organic compounds, we introduced a novel magnetically nickel–copper cytosine complex as a recoverable bimetallic magnetic nano-catalyst for the efficient Pd free C–C and C–N cross coupling reactions (Scheme 1). The heterogeneous bimetallic Fe_3O_4@SiO_2@Cyt-Ni/Cu nanocomposite catalysts the Sonogashira reaction in a short time, lower temperature and low amount of the used catalyst. Catalyst recovery is also easy with an external magnet and can be reused without any further treatment. Highly branched structures due to their multiple internal and external functional groups act as suitable hosts of nanoparticle which lead to the high activity of our catalyst in comparison to the research of Nasresfahani *et al.*[44] The reaction is highly selective, so that no another by-product and/or undesired product was detected in the mixture.

2. Experimental

2.1. Materials and instruments

All materials used in our experiments were purchased from the Sigma Aldrich and Fluca suppliers used without any purification. Progress of the reactions was monitored by thin layer chromatography (TLC). Fourier transform infrared (FT-IR) spectra were recorded with a JASCO FT/IR 4600 spectrophotometer using a KBr pellet. The ^{1}H NMR (400 MHz) and ^{13}CNMR (100 MHz) spectra in the deuterated solvents ($CDCl_3$ and DMSO-d_6) were recorded on a Bruker Avance DPX-250 spectrometer. Field emission scanning electron microscopy (FE-SEM) images were obtained on a SEM FEI Quanta 200. The energy dispersive X-ray (EDX) analyses were performed using a FE-SEM, JEOL 7600F apparatus equipped with a spectrometer of energy dispersion of X-ray from Oxford instruments.

The transmission electron microscopy (TEM) microscopic images were achieved on a Philips EM208S microscope operated at 100 kV. The thermogravimetric analysis (TGA) of the samples were performed on a Q600 model from TA company made in USA under nitrogen atmosphere with a heating rate of

10 °C min^{-1}, and in the temperature range of 25–1000 °C. The vibrating sample magnetometer (VSM) curve of the samples was analyzed on a Lake Shore Cryotronics 7407 at room temperature. The inductively coupled plasma (ICP) experiments were conducted using a VARIAN VISTA-PRO CCD simultaneous ICP-OES instrument. The powder X-ray diffraction (PXRD) patterns were obtained on a Rigaku SmartLab instrument. The analysis of X-ray photoelectron spectroscopy (XPS) is a powerful surface-sensitive technique that was used to confirm the chemical composition, and purity of Fe_3O_4@SiO_2@Cyt-Ni/Cu nanocomposites. The measurements of X-rays photoelectron spectroscopy were conducted using a scanning X-ray microprobe (BESTEK, INC) with monochromatic source Al Kα radiation at photon energy 1486.6 eV and current value 10 mA at 15 kV for the binding energy (BE) spectra. The C 1s (carbon 1s) peak at 291.60 eV was used as a reference for the calibration of all the binding energies. The survey or wide energy range scan (low resolution) analysis of the XPS spectrum taken from a Fe_3O_4@SiO_2@Cyt-Ni/Cu nanocomposites sample was measured with a pass energy of 160 eV and step interval (most minor energy division) of 1 eV for the entire sample surface.

2.2. Preparation of Fe_3O_4@SiO_2 core–shell nanoparticles

Core–shell Fe_3O_4@SiO_2 nanoparticles were synthesized according to a previous reported procedure.[55]

In brief, $FeCl_3 \cdot 6H_2O$ (4.809 mmol, 1.3 g), $FeCl_2 \cdot 4H_2O$ (4.526 mmol, 0.9 g) were dissolved in 300 mL of distilled water with vigorous mechanical stirring at 50 °C for 30 min. Then, NaOH (50 ml, 10% by weight) was slowly added to the solution and the solution pH was maintained at 10. The reaction mixture was then stirred at 50 °C for 2 h. The black magnetite was separated by applying an external magnetic field and was rinsed with water and ethanol several times and dried under vacuum at 80 °C for 10 h.

In the next step, for the synthesis of Fe_3O_4@SiO_2, 0.5 g of the synthesized Fe_3O_4 NPs was dispersed in a mixture containing ethanol (20 mL) and deionized water (20 mL) for 30 min. Then, a mixture of Tetraethyl orthosilicate (1 mL) in ethanol (10 ml) and NaOH (0.5 ml, 10% by weight) was added dropwise and the resultant mixture was stirred for 2 h. The resulting Fe_3O_4@SiO_2 NPs were collected by an external magnet, washed with distilled water and ethanol, and dried in a vacuum oven at 80 °C for 10 h.

2.3. Preparation of (Fe_3O_4@SiO_2-APTES)

At first, Fe_3O_4@SiO_2 (1 g) was dispersed into 20 ml dry toluene for 1 hour. Then, a mixture of 3-aminopropyltriethoxysilane (APTES, 1 ml), 10 ml dry toluene and Et_3N (0.3 ml) as base were dropped into the above solution to the resulting suspension and the mixture was refluxed under argon atmosphere, at 110 °C for 48 h. Following, the obtained Fe_3O_4@SiO_2-NH_2 was separated by an external magnet and washed with toluene, and was dried under vacuum.

2.4. Preparation of Fe_3O_4@SiO_2@TCT

In a typical procedure, Fe_3O_4@SiO_2-NH_2 NPs (0.5 g) were dispersed in toluene (30 mL) and mixed with a solution of TCT (Cyanuric chloride) (1.22 mmol, 0.225 g) in toluene. The obtained mixture was then refluxed at 110 °C for 20 h. Upon completion of the reaction, the solid was separated with assistance of external magnet, rinsed with toluene and was dried at room temperature.

2.5. Preparation of Fe_3O_4@SiO_2@TCT-cytosin

A mixture of cytosine (1.8 mmol, 0.2 g) and Fe_3O_4@SiO_2@TCT (0.5 g) in toluene was stirred under argon atmosphere at 110 °C for 20 h. The volatiles were removed under vacuum and the residue was thoroughly washed with toluene.

2.6. Preparation of copper(II) and nickel(II) immobilized on Fe_3O_4@SiO_2@TCT-cytosin

To prepare Fe_3O_4@SiO_2@Cyt-Ni/Cu nanocomposite, the Fe_3O_4@SiO_2@TCT-cytosin (0.5 g) was dispersed in ethanol (40 mL) and the suspension was stirred for 30 min at RT. Then, mixed with 0.05 g (0.212 mmol) of $Cu(OAC)_2 \cdot 3H_2O$ and 0.05 g (0.200 mmol) of Ni $(OAC)_2 \cdot 4H_2O$. The reaction mixture was then refluxed at 80 °C for 20 h. Afterwards, the precipitate was filtered, washed four times with ethanol and dried.

2.7. General procedure for the Sonogashira coupling reactions using the Fe_3O_4@SiO_2@Cyt-Ni/Cu nanocomposite

A mixture of phenyl acetylene (1.2 mmol), aryl halide (1.0 mmol), the magnetic nanocatalyst (Fe_3O_4@SiO_2@Cyt-Ni/Cu nanocomposite; 10 mg, 0.1 mol% Cu, 0.1 mol% Ni), K_2CO_3 (2.0 mmol), DMSO (3 mL) was heated at 90 °C in an oil bath. The progress of the reaction was screened by TLC at different time intervals. After the completion of the reaction, the reaction mixture was cooled down to room temperature and the catalyst was separated by an external magnetic field. Then, the residual mixture was diluted and the organic layer was extracted with ethyl acetate and water, dried over anhydrous $MgSO_4$, and the solvent was removed under reduced pressure.

The remainder was purified by silica gel plate chromatography to give the desired pure coupling products in high to excellent isolated yields (*n*-hexane : EtOAc = 10 : 0).

2.8. General procedure for C–N cross-coupling

A mixture of *N*-heterocycle (1 mmol), aryl halide (1.2 mmol), Fe_3O_4@SiO_2@Cyt-Ni/Cu nanocomposite (10 mg, 0.1 mol% Cu, 0.1 mol% Ni) and NaOH as a base was added to 2 mL of water and the mixture was stirred at 70 °C. The progress of reaction was monitored by TLC at different time intervals. After the completion of the reaction, the magnetic catalyst was separated by an external magnetic field. Then, the residual mixture was extracted with ethyl acetate and water, dried over anhydrous $MgSO_4$, and finally the resulting crud product was purified by silica gel plate chromatography (*n*-hexane : EtOAc = 10 : 2).

3. Results and discussion

The method of preparing a new recycling Fe_3O_4@SiO_2@Cyt-Ni/Cu catalyst was shown in Scheme 2. Silica-coated magnetite

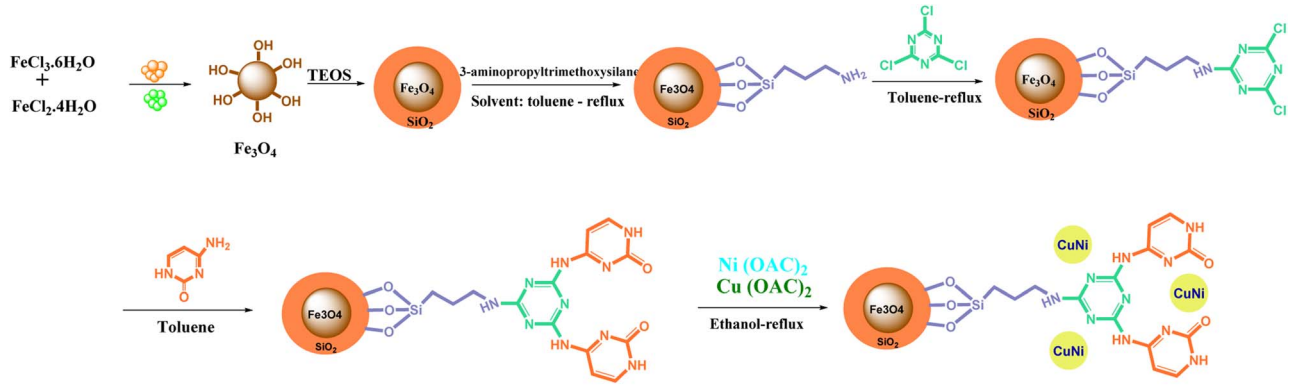

Scheme 2 Synthesis route for a new recycling Fe_3O_4@SiO_2@Cyt-Ni/Cu nanocomposite.

nanoparticles (Fe_3O_4@SiO_2) were prepared according to our previous report.[56] The activated silica was reacted with 3-aminotrimethoxysilane to obtain the functionalized MNPs. This was followed by condensation with cyanuric chloride and cytosine, respectively, by nucleophilic substitution. Subsequently, copper(II) and nickel(II) were stabilized on modified magnetic support to gain the final catalyst. The structure of prepared catalyst was well characterized by the following instrumental techniques: FT-IR, PXRD, TEM, FE-SEM, EDX, TGA, VSM, XPS and density functional theory (DFT).

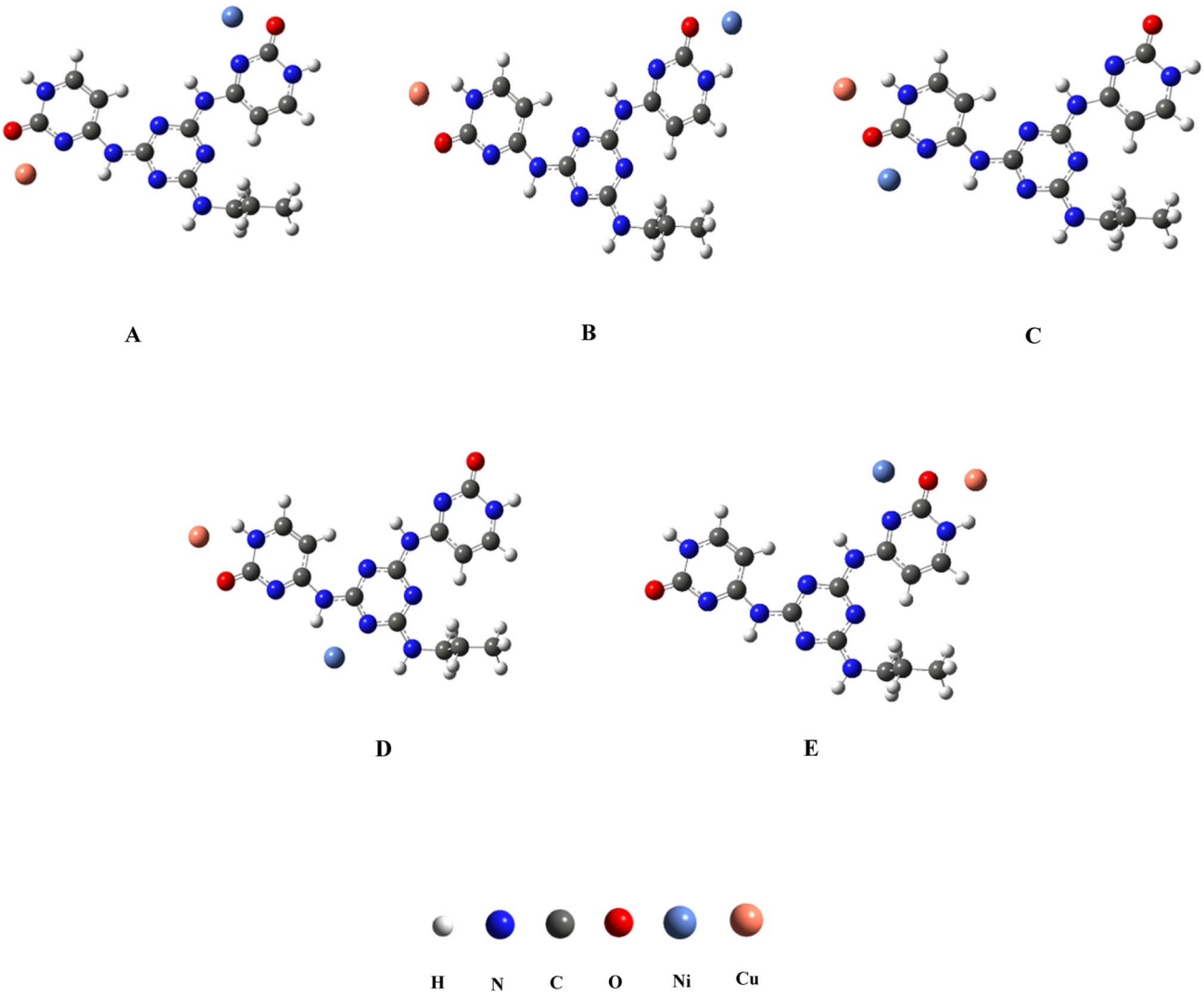

Fig. 1 The different binding modes of Cu and Ni ions with Cyt-Ni/Cu complex.

3.1. Computational study

Density functional theory calculation using the Becke, 3-parameter, -Lee-Yang-Parr (B3LYP) functional[57] was used for the geometry optimization of the possible molecular coordination modes for the bimetallic complexes. The split-valence basis set 6-31G** was applied to oxygen, carbon, nitrogen and hydrogen atoms while the Los Alamos relativistic effective core potential plus DZ basis set (LanL2DZ)[58] basis set was used for Cu and Ni atoms. DFT calculations were carried out using Gaussian 2003 software in the gas phase.[59] The predicted binding modes of Cu and Ni atoms with Cyt-Ni/Cu complex were shown in Fig. 1. In these structures, the interactions of Cu^{2+} and Ni^{2+} with positions on Cyt-Ni/Cu complex which encompass nitrogen and oxygen atoms were considered. The bond lengths of Cu⋯O were in the range of 1.773–1.915 Å, whereas those of Ni⋯O and Ni⋯N ranged from 1.790 to 2.054 Å and from 1.955 to 2.053 Å, respectively (see Table 1). The order of the relative energies for the considered complexes (in a.u.) was: A > E > D > C > B. Based on the obtained results, the molecular structure A was more stable than other studied structures.

3.2. Catalyst characterizations

The catalyst, Fe_3O_4@SiO_2@Cyt-Ni/Cu, was characterized step by step by FT-IR analysis to investigate its structure and formation of the desired bands. The FT-IR spectrum of Fe_3O_4@SiO_2@Cyt-Ni/Cu was shown in Fig. 2. In Fig. 2a, the bond located at 579 cm^{-1} related to Fe–O bond.[60] Stretching vibrations of Fe–O, Si–O–Si (Symm.) and Si–O–Si (Asymm) were demonstrated at the three main bonds at 793, 1074 and 3397 cm^{-1}, respectively, confirming the successful silica coating of Fe_3O_4 nanoparticles.[60]

The absorption bonds at 2800–3000 cm^{-1} and 3200–3500 cm^{-1} (Fig. 2c) were related to the presence of aliphatic C–H and N–H, respectively.[61] The presence of a C–N and C–C bonds in heterocyclic rings were shown at 1500–1600 cm^{-1} and 1463 cm^{-1}, respectively, that strongly supported the preparation of Fe_3O_4@SiO_2@TCT (Fig. 2d). In Fig. 2e, the absorption bond at 1660 cm^{-1} was attributed to the stretching vibration of C=N. Finally, the carbonyl bond in the cytosine structure was detected at 1700 cm^{-1}, confirming the successful functionalization of cytosine on Fe_3O_4@SiO_2-TCT.[62]

Table 1 The intermolecular interaction of metal ions with Cyt-Ni/Cu complex (Å) and relative energy (in atomic unit, a.u.) of the metal complexes at B3LYP approach

Model	Cu⋯O	Cu⋯N	Ni⋯O	Ni⋯N	Energy
A	1.915	2.061	1.899	2.053	−4388.12
B	1.792	—	1.790	—	−4388.04
C	1.808	—	2.054	1.955	−4388.04
D	1.773	—	—	1.974	−4388.06
E	1.808	—	2.025	1.957	−4388.02

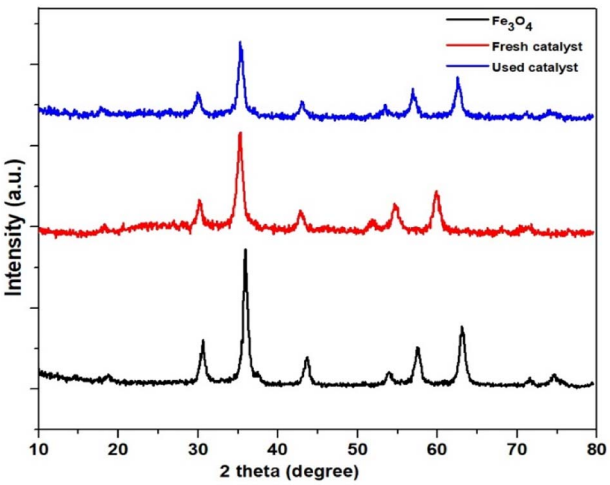

Fig. 3 PXRD patterns of Fe_3O_4 NPs and Fe_3O_4@SiO_2@Cyt-Ni/Cu complex nanocomposite fresh and after reused.

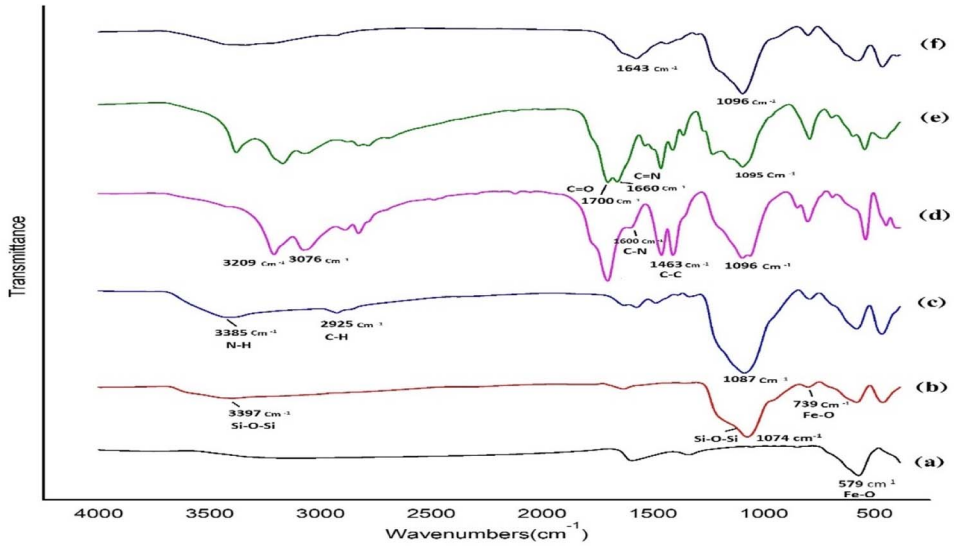

Fig. 2 FT-IR of (a) Fe_3O_4 NPs (b) Fe_3O_4@SiO_2 (c) Fe_3O_4@SiO_2-NH_2 (d) Fe_3O_4@SiO_2@TCT (e) Fe_3O_4@SiO_2@TCT-Cyt (f) Fe_3O_4@SiO_2@Cyt-Ni/Cu.

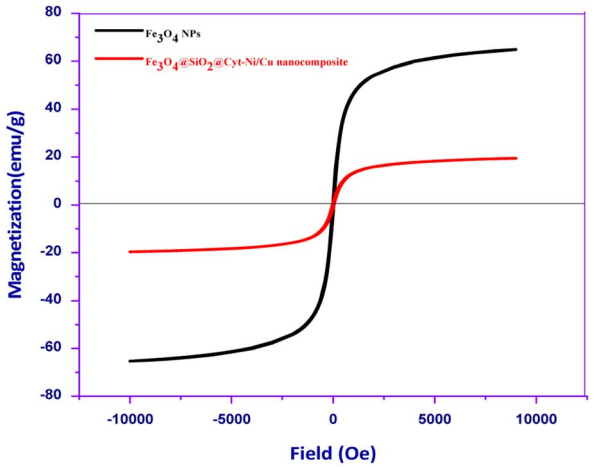

Fig. 4 Magnetization curves for Fe_3O_4 and Fe_3O_4@SiO_2@Cyt-Ni/Cu complex nanocomposite.

Fig. 3 shows PXRD patterns of Fe_3O_4 NPs, Fe_3O_4@SiO_2@Cyt-Ni/Cu nanocomposite fresh and after re-used. The PXRD pattern for Fe_3O_4 was characterized by six specific peaks with strong intensities at $2\theta = 30.1°$, 35.4°, 42.1°, 53.4°, 57.0°, and 62.0° related to (220), (311), (400), (422), (511), and (440) planes, which demonstrated the crystalline cubic inverse spinel structure of Fe_3O_4. In addition, as shown in Fig. 3, PXRD patterns of the synthesized Fe_3O_4 and Fe_3O_4@SiO_2@Cyt-Ni/Cu complex nanocomposite displayed the strong similar diffraction peaks to those of the present Fe_3O_4 NPs.[56] This result showed that the crystal structure of Fe_3O_4 nanoparticles is preserved during silica coating and functionalization of the nanoparticle surface which indicates the successful synthesis of the core shell nanoparticles. A broad peak was observed at low diffraction angle ($2\theta = 10$–25°) in the PXRD pattern of Fe_3O_4@SiO_2@Cyt-Ni/Cu complex nanocomposite, which was related to the amorphous state SiO_2 and cytosine-Ni/Cu complex shells.[63] The results also exhibited that the crystal structure of the nanocatalyst did not change after being used in the reaction. Moreover, using PXRD analysis, size of the nanoparticles was calculated by Scherrer's equation: $D = K\gamma/\beta\cos\theta$, where K is a constant ($K = 0.9$ for Cu Kα), D is the average diameter in Å, β is the broadening of the diffraction line measured at half of its maximum intensity in radians, γ is the wavelength of the X-rays,

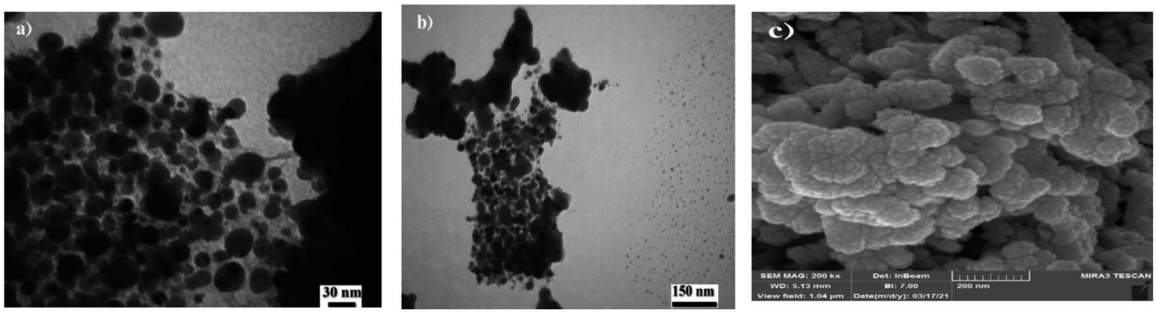

Fig. 5 (a) and (b) TEM, (c) FE-SEM images of Fe_3O_4@SiO_2-Cyt-Ni/Cu nanocomposite.

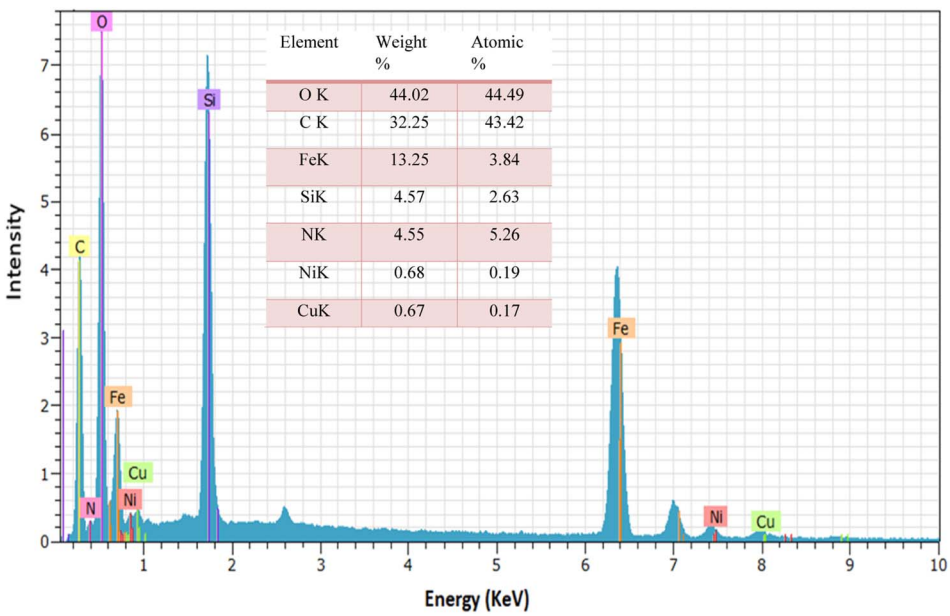

Fig. 6 EDX analysis of Fe_3O_4@SiO_2@Cyt-Ni/Cu complex nanocomposite.

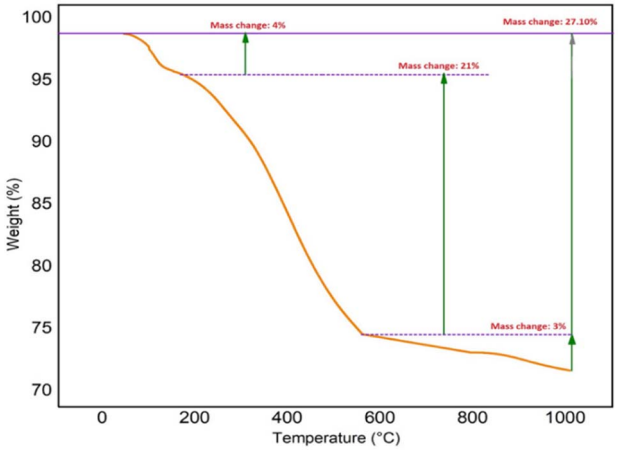

Fig. 7 TGA curves of Fe_3O_4@SiO_2@Cyt-Ni/Cu complex nanocomposite.

and θ is the Bragg diffraction angle. The particle sizes of Fe_3O_4@SiO_2@Cyt-Ni/Cu nanocomposite calculated using the Scherrer equation were about of 24 nm.

The magnetic behavior of Fe_3O_4 and Fe_3O_4@SiO_2@Cyt-Ni/Cu complex nanocomposite was investigated with the vibrating sample magnetometer (VSM) (Fig. 4). The Fe_3O_4 nanoparticles exhibited almost zero coercivity and remanence with no hysteresis loop, approving the high permeability in magnetization and good magnetic responsiveness. Magnetic measurements showed saturation magnetization values of 64.7 and 19.3 emu g^{-1} for Fe_3O_4 and Fe_3O_4@SiO_2@Cyt-Ni/Cu complex nanocomposite, respectively. The results showed that the magnetization of Fe_3O_4 decreases after coating of silica–shell or Cyt-Ni/Cu complex on its surface, indicating the successful immobilization of the Cyt-Ni/Cu complex on Fe_3O_4. However, the behavior of magnetic bimetallic nanoparticles was sufficient to complete the separation from the mixture under an externally applied magnetic field which indicated the magnetic nature of the synthesized catalyst.

The morphology as well as the size of the Fe_3O_4@SiO_2@Cyt-Ni/Cu complex nanocomposite were investigated by FE-SEM and TEM (Fig. 5). The transmission electron microscopy images showed clearly spherical particles which completely dispersed in the catalyst matrix (Fig. 5a and b). The size distribution of Fe_3O_4 nanoparticles was about 21 nm. As can be seen in Fig. 5c, the FE-SEM micrographs clearly showed the distribution of particles in the surface of catalyst. Field emission scanning electron microscopy (FE-SEM) image in Fig. 5c illustrated spherical external morphologies of the catalyst.

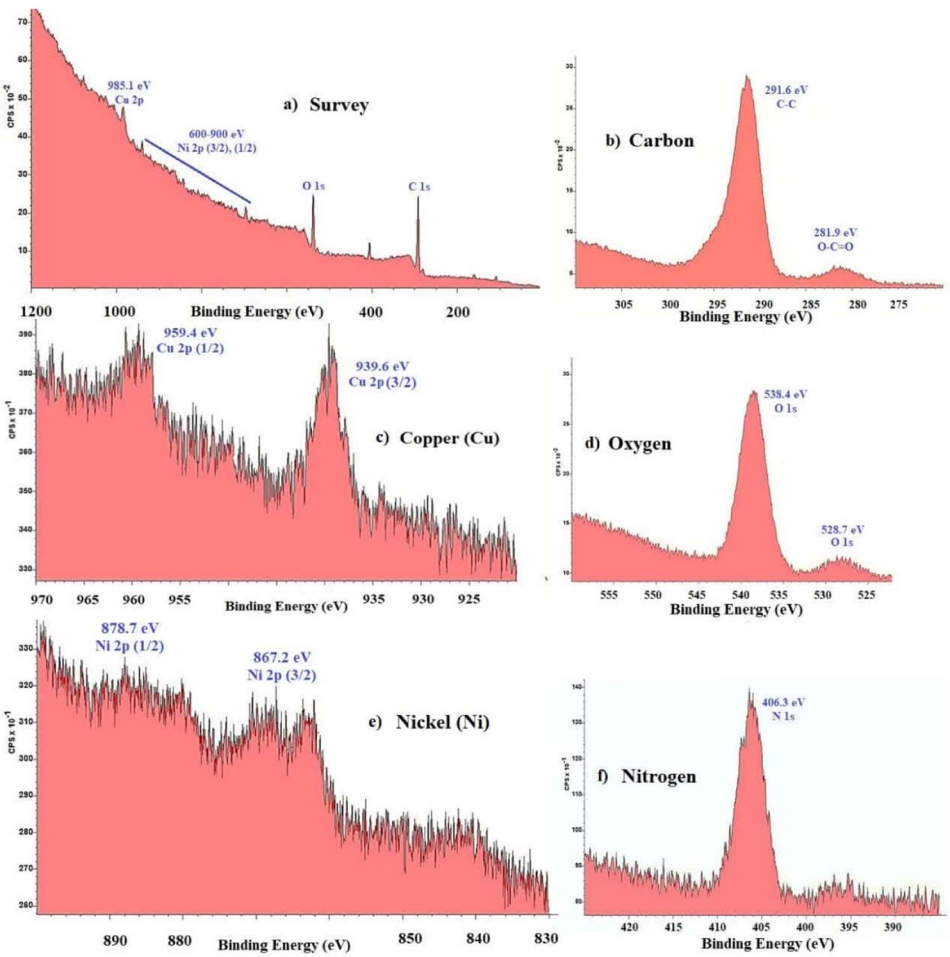

Fig. 8 XPS analysis of Fe_3O_4@SiO_2@Cyt-Ni/Cu nanocomposites (a) survey scan (b) carbon; (c) copper; (d) oxygen; (e) nickel and (f) nitrogen.

Table 2 Optimization of the Sonogashira reaction parameters of 4-iodotoluene and phenylacetylene catalyzed by Fe_3O_4@SiO_2@Cyt-Ni/Cu complex[a]

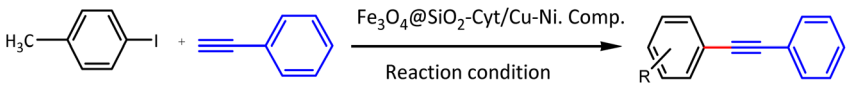

Entry	Cat. amount (mg)	Solvent	Base	Tem. (°C)	Yield[b] (%)
1	10	DMF	Et_3N	90	85
2	10	DMSO	Et_3N	90	87
3	10	H_2O	Et_3N	90	Trace
4	10	EtOH	Et_3N	90	Trace
5	10	CH_3CN	Et_3N	90	70
6	10	CH_2Cl_2	Et_3N	90	50
7	10	THF	Et_3N	90	60
8	10	DMSO	K_2CO_3	90	93
9	10	DMSO	NaOH	90	40
10	10	DMSO	K_3PO_4	90	90
11	10	DMSO	KOH	90	68
12	10	DMSO	K_2CO_3	R.T.	50
13	10	DMSO	K_2CO_3	80	90
14	10	DMSO	K_2CO_3	100	94
13	8	DMSO	K_2CO_3	90	88
14	20	DMSO	K_2CO_3	90	92
15	30	DMSO	K_2CO_3	90	89

[a] Reaction conditions: 4-iodotoluene (1 mmol), phenyl acetylene (1.2 mmol), base (2 mmol), in solvent (3 mL) for 2 h. [b] Isolated yield.

The energy dispersive X-ray spectroscopy analysis was performed to investigate the component of the composite particles in the catalyst. The EDX results of Fe_3O_4@SiO_2@Cyt-Ni/Cu complex nanocomposite showed that the elements such as carbon, nitrogen, oxygen, iron, copper and nickel are present in the structure of the catalyst (Fig. 6).

The bimetallic catalyst was confirmed in the presence of copper and nickel elements with weight percentages of 0.67 and 0.68, respectively. ICP analysis of the Fe_3O_4@SiO_2@Cyt-Ni/Cu complex nanocomposite showed 0.60% W Cu and 0.63% W Ni on the catalyst in agreement with the EDX results.

The thermal behavior of the Fe_3O_4@SiO_2@Cyt-Ni/Cu complex nanocomposite was characterized by TGA analysis as shown in Fig. 7. The corresponding TGA spectrum illustrated good thermal stability and three weight loss steps totaling 27.10%, which in the first step of decomposition, 4% weigh loss was observed in the region of 90–220 °C, which is attributed to the loss of physically adsorbed solvent and surface hydroxyl group.[64] The second significant weight loss (21%) occurred between 220 °C and 560 °C which can be directly related to the decomposition of different organic compounds on the nanoparticles surface. The third weight loss (3%) at the temperature range of 560–1000 °C was attributed to the oxidation of metals in the structure of Fe_3O_4@SiO_2@Cyt-Ni/Cu complex nanocomposite.[65] Fig. 8a shows XPS wide scan spectra (survey spectrum) of Fe3O4@SiO2@Cyt-Ni/Cu nanocomposites, which have confirmed that the peaks are associated with the elements of nickel (Ni), copper (Cu), oxygen (O), and carbon (C). Fig. 8b, d and f show the high-resolution spectra (core XPS spectra) of C 1s, O 1s, and F 1s, respectively. The XPS results in Fig. 8c is the core level or narrow energy range spectra of Cu 2p showing the main shake-up peak at the higher binding energy side of the Cu 2p (3/2) and suggesting the existence of Cu 2p (1/2). Furthermore, in the Fig. 8e core level spectra of Ni 2p, the peaks at 878.7 eV and 867.2 eV could be assigned to Ni 2p (1/2) and Ni 2p (3/2) respectively.

3.2.1 Optimization of reaction parameters. The coupling reaction between 4-iodotoluene and phenylacetylene was performed as a model to study the optimized reaction parameters and the effect of solvent, base, temperature and amount of catalyst on the reaction efficiency.

In the first step, the influence of different solvent was checked. Solvents such as DMF and DMSO, which are polar-aprotic solvents, can have high efficiencies of about 85–87%. We chose DMSO solvent as the best solvent.

Different base such as K_3PO_4, K_2CO_3, KOH, Et_3N and NaOH were examined in Sonogashira reaction and K_2CO_3 was the most effective base. The temperature effect was screened on the model reaction of 4-iodotoluene and phenylacetylene at different temperatures in DMSO, K_2CO_3 as a base, which the corresponding data was presented in Table 2. The best yield of the desired product was obtained at a temperature of 90 °C; so that the reaction had a yield of 50% at room temperature.

Further, we was checked the influence of different amount of the catalyst on the efficiency of the cross-coupling reaction. The best result was provided when 0.1 mol% of the catalyst is employed in the model reaction. The model reaction was tested in the absence of the catalyst, but the product was not formed, indicating the key role of the catalyst in the reaction medium.

Table 3 Catalyzed Sonogashira reaction of 4-iodotoluene and phenylacetylene by Fe_3O_4@SiO_2@Cyt-Ni/Cu complex nanocomposite[a]

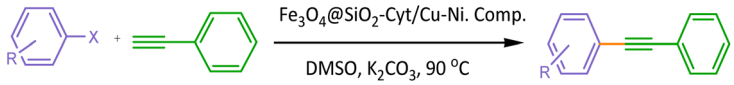

Entry	Aryl halide	Product	Time (h)	Yield[b] (%)
1	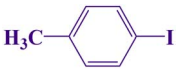	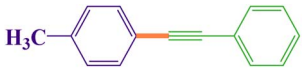	2	93
2		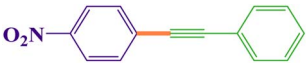	1	96
3	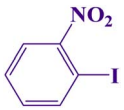	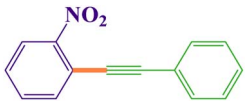	1.5	90
4	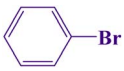		2	83
5	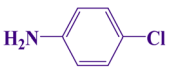	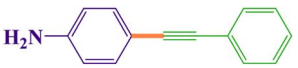	3.5	80
6	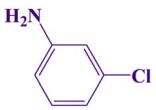	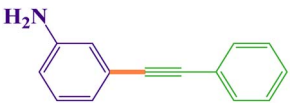	4	75
7	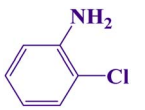	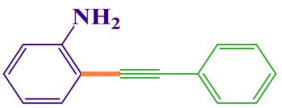	4	72
8	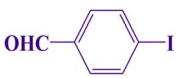	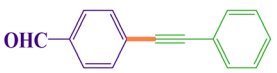	1.5	83
9	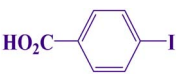	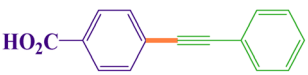	1.5	80
10	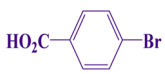	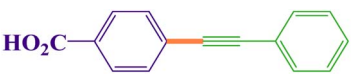	2.5	75
11	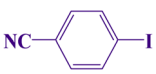	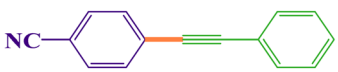	2	97
12		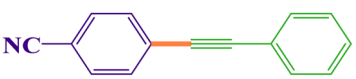	2.5	95

[a] Reaction conditions: 4-iodotoluene (1 mmol), phenyl acetylene (1.2 mmol), K_2CO_3 (2 mmol), DMSO (3 mL), 90 °C. [b] Isolated yield.

Thus, the optimized conditions were selected to be 90 °C, K_2CO_3 (as base), DMSO (as solvent), and 10 mg of the catalyst (0.1 mol% of Ni/Cu) (Table 2, entry 8).

In optimal conditions, the efficiency of the Fe_3O_4@SiO_2@-Cyt-Ni/Cu complex nanocomposite in the Sonogashira coupling reaction was investigated by a variety of aryl halides with phenylacetylene (Table 3).

According to the satisfactory results of the Sonogashira reaction, we decided to evaluate the efficiency of the catalytic activity of Fe_3O_4@SiO_2@Cyt-Ni/Cu complex nanocomposite into C–N cross-coupling reaction of on aryl halides or phenylboronic acid with *N*-heterocycles (Table 4). The C–N cross-coupling reaction was performed in the presence of pheylbronic acid or variety of aryl halides with *N*-heterocycles compounds in water (2 mL), NaOH (1 mmol) in the presence of catalyst (10 mg, 0.1 mol% Ni/Cu) at a constant time at 70 °C.

3.2.2 Control experimental. We investigated the advantage and synergistic effects of the model reactions in the presence of various parts of catalyst as control experimental. The results showed in Table 5. As shown in the table, in the presence of Fe_3O_4 NPs, Fe_3O_4@SiO_2, Fe_3O_4@SiO_2-NH_2 and Fe_3O_4@SiO_2-NH_2-TCT, no coupling product was observed under the reaction

Table 4 Catalyzed C–N coupling reaction of aryl halide/phenylboronic acid with *N*-heterocycles by Fe_3O_4@SiO_2@Cyt-Ni/Cu complex nanocomposite[a]

Entry	Aryl halide or phenyl bronic acid	*N*-Heterocyclic Compound	Product	Yield[b] (%)
1		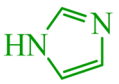	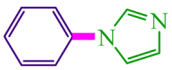	90
2	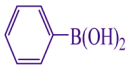		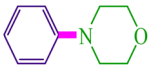	78
3			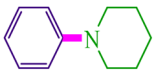	83
4	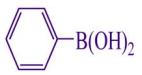	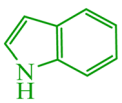	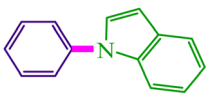	—
5	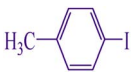	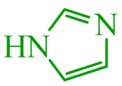	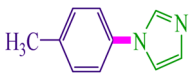	78
6	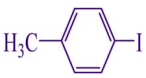		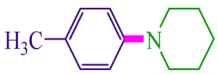	85
7	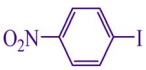	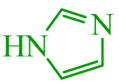		80
8	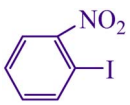	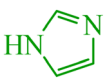	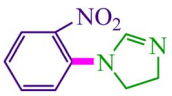	20

[a] Reaction conditions: aryl halide or phenyl bronic acid (1.2 mmol), *N*-heterocycles compounds (1 mmol), NaOH (1 mmol) in 2 mL water for 2 h. [b] Isolated yield.

Table 5 Designed control experiments for Sonogashira cross-coupling[a]

Entry	Catalyst	Yield[b] (%)
1	Fe_3O_4 NPs	0
2	Fe_3O_4@SiO_2	0
3	Fe_3O_4@SiO_2-NH_2	0
4	Fe_3O_4@SiO_2-NH_2-TCT	Trace
5	Fe_3O_4@SiO_2-NH_2-TCT-Cyt	Trace
6	Fe_3O_4@SiO_2-NH_2-TCT-Cyt-Ni	50
7	Fe_3O_4@SiO_2-NH_2-TCT-Cyt-Cu	65
8	Fe_3O_4@SiO_2@Cyt-Ni/Cu	93
9	$Ni(OAc)_2 \cdot 4H_2O$	Trace
10	$Cu(OAc)_2 \cdot H_2O$	Trace

[a] Reaction conditions: aryl halide (1 mmol), phenylacetylene (1.2 mmol), cat. (0.01 g), DMSO (3 mL), K_2CO_3 (2 mmol), 90 °C, 2 h. [b] Isolated yield.

conditions. The Fe_3O_4@SiO_2-NH_2-TCT-Cyt demonstrated no significant efficiency of catalytic activity (about 5–10% yield). In addition, the catalytic effect of the nickel and copper salt was evaluated and no considerable product observed in the Sonogashira model reaction. In the next step, the synergistic effect of the two encoded metals was investigated. By coordinating of copper center only, the efficiency of catalytic activity was increased to 65% in the coupling reaction. The high efficiency was achieved by coordinating copper and nickel metals and forming a bimetallic catalytic system. The strong synergistic effect between Cu and Ni provides better catalytic activity in the Sonogashira coupling reaction. To confirm the efficiency of the catalytic of the Fe_3O_4@SiO_2@Cyt-Ni/Cu nanocomposite for C–C and C–N coupling reactions, a comparative table (Table 6) of other literature was prepared. Of the advantages of Fe_3O_4@SiO_2@Cyt-Ni/Cu nanocomposite that makes this catalyst better than the other catalysts is high efficiency, short time and easy recycling.

3.2.3 Mechanism study. A plausible mechanism could be proposed for the Fe_3O_4@SiO_2@Cyt-Ni/Cu nanocomposite catalyzed the Sonogashira coupling reaction, as shown in Scheme 3(A). As depicted in Scheme 3, the reaction probably proceeds through Ni–Cu catalytic cycles. According to the results obtained in control reactions, the simultaneous presence of metal centers which results in a synergistic effect and a significant increase in efficiency can also be attributed to this effect.

In nickel catalysis (Ni cycle), fast oxidative addition occurs between C–X in aryl halide with the Ni center in the Fe_3O_4@SiO_2@Cyt-Ni/Cu nanocomposite surface to form ArNiX species

Table 6 The comparison of the activity of Fe_3O_4@SiO_2@Cyt-Ni/Cu complex nanocomposite with some reported catalysts

Entry	Reaction	Catalyst	Temp. (°C)	Solvent/base	Time (h)	Yield (%)	Ref.
1	**Sonogashira**[a]	**Fe_3O_4@SiO_2@Cyt-Ni/Cu (0.1 mol%)**	**90**	**DMSO/K_2CO_3**	**2**	**93**	**This work**
2		MNPs@Cs-MS-Co (0.55 mol%)[b]	140	DMSO/KOH	10	72	60
3		γ-Fe_2O_3@Cu(II)IL-SB (0.4 mol%)	90	DMSO/K_2CO_3	4	93	66
4		PdCu@GQD@Fe_3O_4(Pd 0.3 mol%, Cu 0.35 mol%)	60	Toluene/DABCO	24	99	67
5		SiO_2@Fe_3O_4-Pd (1 mol%)	100	DMF/K_2CO_3	6	95	68
6	**C–N coupling**[c]	**Fe_3O_4@SiO_2@Cyt-Ni/Cu (0.1 mol%)**	**70**	**Water/NaOH**	**1**	**90**	**This work**
7		CuNps/TiO_2 (1.6 mol%)	120	DMF/Cs_2CO_3	16	99	69
8		Amide-based pincer nickel(II) (0.2 mol%)	110	DMSO/KO^{t}Bu	3	97	70
9		Fe_3O_4@PEG/Cu-Co (0.47 mol% Cu, 0.17 mol% Co)	90	Water/—	6.5	80	71

[a] Sonogashira reaction of 4-iodotoluene and phenylacetylene. [b] MNPs@Cs-MS-Co: cobalt tagged on MNPs-chitosan functionalized with methyl salicylate. [c] C–N coupling reaction of aryl halide or phenyl bronic acid and *N*-heterocycles compounds.

and subsequent connection with a cocatalytic cycle involving Cu (Cu cycle).

The copper cyclization (right part in Scheme 3), involves the formation of a π complex between the phenyl acetylene and copper sites on the catalyst, followed by the formation of a copper-acetylide intermediate in the presence of base.

Next, by another connection with the nickel cycle, the RNi(–C≡CPh) species is attained through a transmetalation reaction which gives the final coupled alkyne after reductive elimination accompanied by regeneration of the nickel catalyst.[44,72,73]

As similar possible mechanism proposed for C–N coupling reaction (B). In this mechanism, the active Cu complex attacks the amine group. Then, the amine proton is removed by base and the amine–copper intermediate is formed (Cu cycle). In the nickel catalytic cycle, the aryl halide is close to the active nickel of the catalyst surface and oxidative addition causes the formation of RNiX intermediate. After coupling the two cycles, the desired coupled product is obtained through a reductive elimination reaction during a transmetalation reaction.[71]

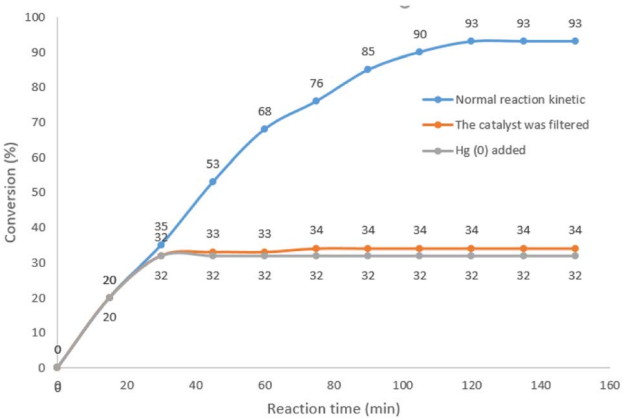

Fig. 9 Reaction kinetics, Hg(0) poisoning, and hot filtration studies for the Sonogashira coupling reaction of 4-iodotoluene and phenylacetylene catalyzed by Fe_3O_4@SiO_2@Cyt-Ni/Cu nanocomposite in DMSO.

3.2.4 Recyclability studies. Easy work-up and reusability of a catalyst are key aspects for environmental and practical destinations. Therefore, reusability of the Fe_3O_4@SiO_2@Cyt-Ni/Cu nanocomposite examined for the Sonogashira model reaction under optimized conditions. The catalyst easily was recovered by an external magnet from the reaction solution, washed with water and ethanol, dried and reused for 7 runs without a significant reactivity loss (Fig. 10).

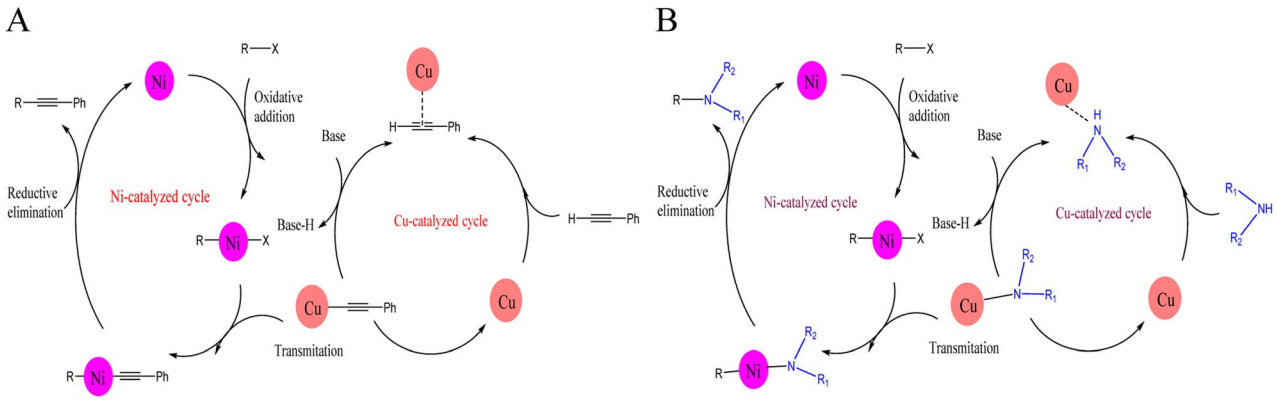

Scheme 3 A plausible reaction mechanism for (A) Sonogashira cross-coupling reaction and (B) C–N cross-coupling reaction catalyzed by Fe_3O_4@SiO_2@Cyt-Ni/Cu nanocomposite.

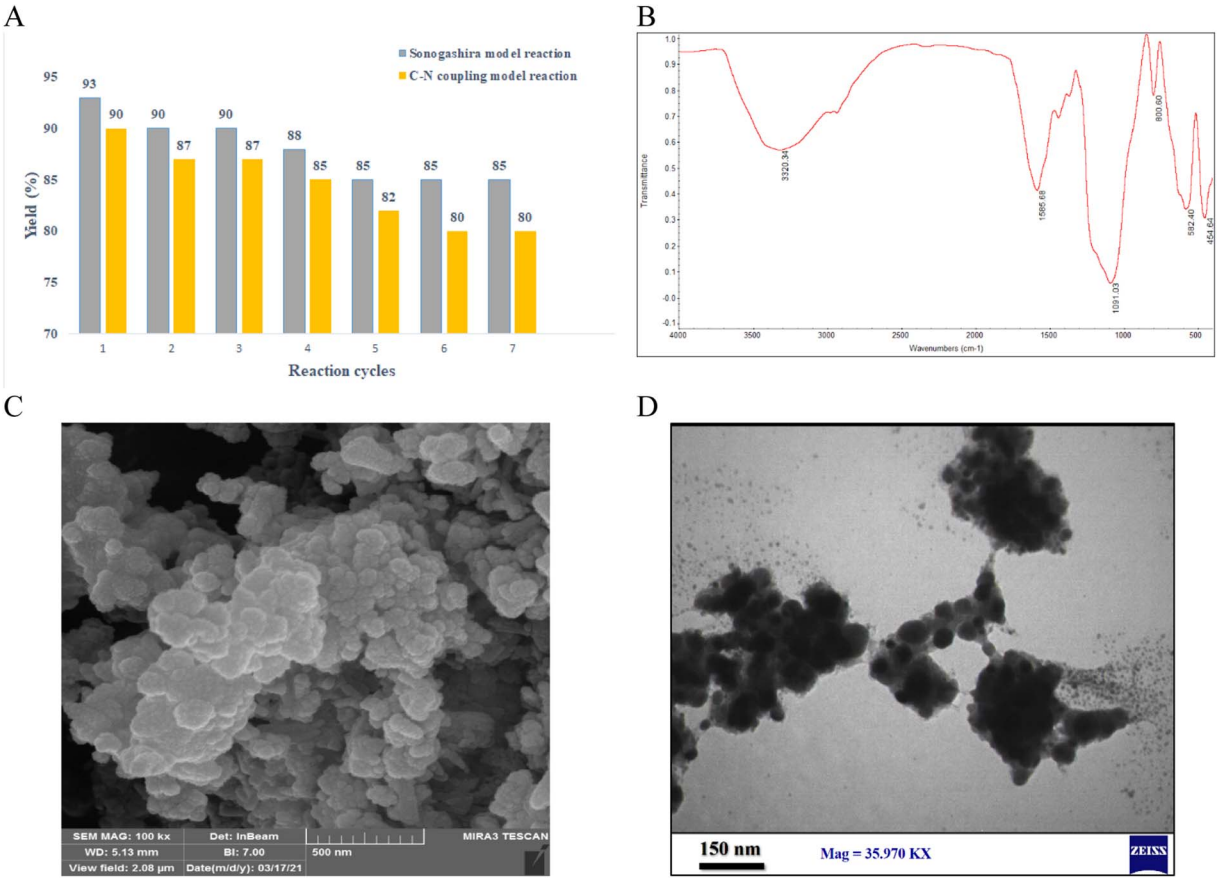

Fig. 10 (A) Recovery and reusability of Fe_3O_4@SiO_2-Cyt-Ni/Cu nanocomposite in the Sonogashira and C–N cross-coupling reaction under optimized reaction conditions (B) FT-IR spectrum, (C) FE-SEM, and (D) TEM images of the recovered catalyst after the 7th run.

In order to elucidate the heterogeneous nature of the catalyst, two tests including Hg(0)-poisoning and hot filtration were studied on the model Sonogashira reaction in optimized conditions. In hot filtration test, the catalyst was magnetically removed in 32% of conversion (GC) after 30 min and then the reaction was allowed to proceed. The conversion reached 34% after 2.5 h of reaction, indicating the heterogeneous performance of the catalyst in the reaction medium. This confirmed that only negligible leaching occurred in recycle and leaching studies (Fig. 9).

Second, the mercury poisoning experimental was carried out in the optimized model reaction. After 30 min of the reaction (yield: 35%), the catalyst was poisoned by addition of Hg(0) and the reaction stopped immediately. This result clearly indicated the heterogeneous nature of the catalyst in the reaction condition (Fig. 9).

4 Conclusion

In this work, Fe_3O_4@SiO_2@Cyt-Ni/Cu as a bimetallic heterogeneous nanocatalyst was successfully synthesized and characterized by different techniques such as FT-IR, PXRD, EDX, VSM, TEM, FE-SEM, XPS and TGA analyses and DFT study. Fe_3O_4@SiO_2@Cyt-Ni/Cu nanocomposite catalyzed the C–C and C–N cross-coupling reaction with high yields in short reaction times. The bimetallic catalyst showed a better activity than analogous monometallic Cu and Ni catalysts, which could be attributed to synergetic effect between the two metals. This reported method had significant advantages in term of using low amount of the catalyst, easy separation of catalyst, recyclability and reusability of the catalyst without a notable decrease in catalytic activity.

Conflicts of interest

There are no conflicts to declare.

Acknowledgements

The authors are grateful to the University of Birjand for its financial support.

Notes and references

1 J. Magano and J. R. Dunetz, *Chem. Rev.*, 2011, **111**, 2177–2250.
2 C. Torborg and M. Beller, *Adv. Synth. Catal.*, 2009, **351**, 3027–3043.
3 P. Devendar, R.-Y. Qu, W.-M. Kang, B. He and G.-F. Yang, *J. Agric. Food Chem.*, 2018, **66**, 8914–8934.

4 J. Hassan, M. Sévignon, C. Gozzi, E. Schulz and M. Lemaire, *Chem. Rev.*, 2002, **102**, 1359.
5 E. Sperotto, G. P. M. van Klink, G. van Koten and J. G. de Vries, *Dalton Trans.*, 2010, **39**, 10338.
6 J. Tan, Y. Bai, X. Zhang, C. Huang, D. Liu and L. Zhang, *Macromol. Rapid Commun.*, 2016, **37**, 1434–1440.
7 C. Jung, M. Krumova and S. Mecking, *Langmuir*, 2014, **30**, 9905–9910.
8 F. F. Wagner and D. L. Comins, *J. Org. Chem.*, 2006, **71**, 8673–8675.
9 K. C. Nicolaou and W. Dai, *Angew. Chem., Int. Ed. Engl.*, 1991, **30**, 1387–1416.
10 N. Matsumi, K. Naka and Y. Chujo, *J. Am. Chem. Soc.*, 1998, **120**, 5112–5113.
11 R. E. Martin and F. Diederich, *Angew. Chem., Int. Ed.*, 1999, **38**, 1350–1377.
12 M. Inouye, K. Takahashi and H. Nakazumi, *J. Am. Chem. Soc.*, 1999, **121**, 341–345.
13 S. H. Chanteau and J. M. Tour, *Tetrahedron Lett.*, 2001, **42**, 3057–3060.
14 M. Aghayee, M. A. Zolfigol, H. Keypour, M. Yarie and L. Mohammadi, *Appl. Organomet. Chem.*, 2016, **30**, 612–618.
15 S. Sheikh, M. A. Nasseri, M. Chahkandi, O. Reiser and A. Allahresani, *RSC Adv.*, 2022, **12**, 8833–8840.
16 M. Ghabdian, M. A. Nasseri, A. Allahresani and A. Motavallizadehkakhky, *Res. Chem. Intermed.*, 2021, **47**, 1713–1728.
17 S. Akay, T. Baran, B. Kayan and D. Kalderis, *Mater. Chem. Phys.*, 2021, **259**, 124176.
18 G. Halligudra, C. C. Paramesh, R. Mudike, M. Ningegowda, D. Rangappa and P. D. Shivaramu, *ACS Omega*, 2021, **6**, 34416–34428.
19 K. Sun, H. Shan, G. P. Lu, C. Cai and M. Beller, *Angew. Chem., Int. Ed.*, 2021, **60**, 25188–25202.
20 A. Rezaeifard, M. Jafarpour, A. Farrokhi, S. Parvin and F. Feizpour, *RSC Adv.*, 2016, **6**, 64640–64650.
21 K. Hemmat, M. A. Nasseri and A. Allahresani, *ChemistrySelect*, 2019, **4**, 4339–4346.
22 A. A. Liori, I. K. Stamatopoulos, A. T. Papastavrou, A. Pinaka and G. C. Vougioukalakis, *Eur. J. Org. Chem.*, 2018, **2018**, 6134–6139.
23 F. Monnier, F. Turtaut, L. Duroure and M. Taillefer, *Org. Lett.*, 2008, **10**, 3203–3206.
24 L. Wang, P. Li and Y. Zhang, *Chem. Commun.*, 2004, 514–515.
25 D. Ma and F. Liu, *Chem. Commun.*, 2004, 1934–1935.
26 M. B. Thathagar, J. Beckers and G. Rothenberg, *Green Chem.*, 2004, **6**, 215–218.
27 M. A. Bhosale, T. Sasaki and B. M. Bhanage, *Catal. Sci. Technol.*, 2014, **4**, 4274–4280.
28 J. Santandrea, A.-C. Bédard and S. K. Collins, *Org. Lett.*, 2014, **16**, 3892–3895.
29 Z. Wang, T. Zheng, H. Sun, X. Li, O. Fuhr and D. Fenske, *New J. Chem.*, 2018, **42**, 11465–11470.
30 J. Yin, W. Chai, F. Zhang and H. Li, *Appl. Organomet. Chem.*, 2013, **27**, 512–518.
31 F. M. Moghaddam, G. Tavakoli and H. R. Rezvani, *Catal. Commun.*, 2015, **60**, 82–87.
32 B. Wang, Y. Wang, X. Guo, Z. Jiao, G. Jin and X. Guo, *Catal. Commun.*, 2017, **101**, 36–39.
33 H. Zhao, B. Huang, Y. Wu and M. Cai, *J. Organomet. Chem.*, 2015, **797**, 21–28.
34 K. Shah, S. Bhagat, D. Varade and S. Singh, *Colloids Surf., A*, 2018, **553**, 50–57.
35 S. Sohni, S. A. Khan, K. Akhtar, S. B. Khan, A. M. Asiri, R. Hashim and A. K. M. Omar, *Colloids Surf., A*, 2018, **549**, 184–195.
36 K. Mallikarjuna and H. Kim, *Colloids Surf., A*, 2017, **535**, 194–200.
37 T. Szumełda, A. Drelinkiewicz, R. Kosydar, M. Góral-Kurbiel, J. Gurgul and D. Duraczyńska, *Colloids Surf., A*, 2017, **529**, 246–260.
38 L. Srisombat, J. Nonkumwong, K. Suwannarat, B. Kuntalue and S. Ananta, *Colloids Surf., A*, 2017, **512**, 17–25.
39 R. K. Rai, D. Tyagi, K. Gupta and S. K. Singh, *Catal. Sci. Technol.*, 2016, **6**, 3341–3361.
40 D. R. Pye and N. P. Mankad, *Chem. Sci.*, 2017, **8**, 1705–1718.
41 D. N. Olekszyszen, B. L. Albuquerque, D. de O. Silva, G. L. Tripodi, D. C. de Oliveira and J. B. Domingos, *Nanoscale*, 2020, **12**, 1171–1179.
42 A. Abolhosseini Shahrnoy, A. R. Mahjoub, S. Shokrollahi, N. Ezzati, K. Elsner and C. T. Koch, *Appl. Organomet. Chem.*, 2020, **34**, 5645.
43 A. Verma and W. L. Santos, *J. Am. Chem. Soc.*, 2016, 313–356.
44 Z. Nasresfahani and M. Z. Kassaee, *J. Organomet. Chem.*, 2021, **937**, 121703.
45 V. Seethapathy, P. Sudarsan, A. K. Pandey, A. Pandiyan, T. V. Kumar, K. Sanjeevi and S. B. K. Moorthy, *New J. Chem.*, 2019, **43**, 3180–3187.
46 M. Nasrollahzadeh, M. Sajjadi, H. Komber, H. A. Khonakdar and S. M. Sajadi, *Appl. Organomet. Chem.*, 2019, **33**, 4938.
47 L. Chen, H. Xu, H. Cui, H. Zhou, H. Wan and J. Chen, *Particuology*, 2017, **34**, 89–96.
48 S. A. Hashemizadeh and M. Biglari, *J. Mater. Sci.: Mater. Electron.*, 2018, **29**, 13025–13031.
49 S. Rana and S. B. Jonnalagadda, *RSC Adv.*, 2017, **7**, 2869–2879.
50 G. H. Mohamed Saeed, S. Radiman, S. S. Gasaymeh, H. N. Lim and N. M. Huang, *J. Nanomater.*, 2010, 1–5.
51 B. H. Lipshutz, D. M. Nihan, E. Vinogradova, B. R. Taft and Ž. V. Bošković, *Org. Lett.*, 2008, **10**, 4279.
52 J. Sun, X. Jin, F. Zhang, W. Hu, J. Liu and R. Li, *Catal. Commun.*, 2012, **24**, 30–33.
53 G. B. B. Varadwaj, S. Rana and K. M. Parida, *RSC Adv*, 2013, **3**(20), 7570–7578.
54 R. Krishna, D. M. Fernandes, J. Ventura, C. Freire and E. Titus, *Int. J. Hydrog.*, 2016, **41**, 11608–11615.
55 M. Kazemnejadi, S. A. Alavi, G. Z. Rezazadeh, M. A. Nasseri, A. Allahresani and M. Esmaeilpour, *Green Chem.*, 2019, **21**, 1718–1734.
56 M. Esmaeilpour, J. Javidi, M. M. Abarghoui and F. N. Dodeji, *J. Iran. Chem. Soc.*, 2014, **11**, 499–510.
57 C. Lee, W. Yang and R. G. Parr, *Phys. Rev.*, 1988, **37**, 785.
58 P. J. Hay and W. R. Wadt, *J. Chem. Phys.*, 1985, **82**, 270.

59 M. J. Frisch, G. W. Trucks, H. B. Schlegel, G. E. Scuseria, M. A. Robb, J. R. Cheeseman, J. A. Montgomery, *et al.*, *Gaussian 03, Revision B. 03*, Gaussian, Inc., Pittsburgh PA, 2003.
60 M. Kazemnejadi, S. A. Alavi, Z. Rezazadeh, M. A. Nasseri, A. Allahresani and M. Esmaeilpour, *J. Mol. Struct.*, 2019, **1186**, 230–249.
61 M. Ghiaci, M. Zarghani, F. Moeinpour and A. Khojastehnezhad, *Appl. Organomet. Chem.*, 2014, **28**, 589–594.
62 F. Rajabi, F. Fayyaz and R. Luque, *Microporous Mesoporous Mater.*, 2017, **253**, 64–70.
63 M. Esmaeilpour, J. Javidi, F. N. Dodeji and M. M. Abarghoui, *Transition Met. Chem.*, 2014, **39**, 797–809.
64 A. R. Sardarian, M. Kazemnejadi and M. Esmaeilpour, *Dalton Trans.*, 2019, **48**, 3132–3145.
65 H. Li, N. Zhao, C. He, C. Shi, X. Du and J. Li, *Mater. Sci. Eng., A*, 2008, **473**, 355–359.
66 M. A. Nasseri, Z. Rezazadeh, M. Kazemnejadi and A. Allahresani, *J. Iran. Chem. Soc.*, 2019, **16**, 2693–2705.
67 M. Gholinejad, J. Ahmadi, C. Nájera, M. Seyedhamzeh, F. Zareh and M. Kompany-Zareh, *ChemCatChem*, 2017, **9**, 1442–1449.
68 M. Gholinejad, J. Ahmadi, C. Nájera, M. Seyedhamzeh, F. Zareh and M. Kompany-Zareh, *ChemCatChem*, 2017, **9**, 1442–1449.
69 A. Y. Mitrofanov, A. V. Murashkina, I. Martín-García, F. Alonso and I. P. Beletskaya, *Catal. Sci. Technol.*, 2017, **7**, 4401–4412.
70 Y. M. Albkuri, A. B. RanguMagar, A. Brandt, H. A. Wayland, B. P. Chhetri, C. M. Parnell and A. Ghosh, *Catal. Lett.*, 2020, **150**, 1669–1678.
71 M. A. Nasseri, Z. Rezazadeh, M. Kazemnejadi and A. Allahresani, *Dalton Trans.*, 2020, **49**, 10645–10660.
72 F. Mohajer, M. M. Heravi, V. Zadsirjan and N. Poormohammad, *RSC Adv.*, 2021, **11**, 6885–6925.
73 X. Wang, Y. Song, J. Qu and Y. Luo, *Organometallics*, 2017, **36**, 1042–1048.